A Letters Journal Exploring the Frontiers of Physics

November 2014

EPL, **108** (2014) 48002
doi: 10.1209/0295-5075/108/48002

www.epljournal.org

Drag reduction, from bending to pruning

D. Lopez[1(a)], C. Eloy[2,3], S. Michelin[1] and E. de Langre[1]

[1] *LadHyX, Département de Mécanique, École Polytechnique - 91128 Palaiseau, France*
[2] *Department of Mechanical and Aerospace Engineering, University of California San Diego 9500 Gilman Drive, La Jolla, CA 92093-0411, USA*
[3] *Aix Marseille Université, CNRS, IRPHE UMR 7342 - 13013 Marseille, France*

received 11 July 2014; accepted in final form 27 October 2014
published online 17 November 2014

PACS 87.10.Pq – Elasticity theory
PACS 89.75.Da – Systems obeying scaling laws
PACS 89.75.Hc – Networks and genealogical trees

Abstract – Most plants and benthic organisms have evolved efficient reconfiguration mechanisms to resist flow-induced loads. These mechanisms can be divided into bending, in which plants reduce their sail area through elastic deformation, and pruning, in which the loads are decreased through partial breakage of the structure. In this letter, we show by using idealized models that these two mechanisms or, in fact, any combination of the two, yield comparable relative reduction in the drag experienced by terrestrial and aquatic vegetation.

Copyright © EPLA, 2014

Introduction. – A major mechanical constraint on terrestrial plants and benthic organisms results from external fluid flows. To resist large flow-induced loads, plants have evolved two types of adaptability. The first one is a long time-scale adaptability, where the flow induces shape modifications of the plants [1,2]. The second one may occur on long or short time-scales and involves time-reversible geometrical changes. This latter mechanism, known as "reconfiguration" [3,4], can itself be divided into two distinct mechanisms: bending and pruning.

In bending, also known as elastic reconfiguration, the body deforms significantly under the flow forces, thereby reducing its drag compared to that of a non-deformable body [5]. Over the past decade, several experimental, theoretical and numerical studies have provided a good understanding of this mechanism [6–10]. Alternatively, in pruning, the sail area is reduced by breaking parts of the plant structure, as may be observed in trees [11,12]. Like bending, pruning leads to significant drag reduction. The parts of the plant removed by flow-induced pruning can be either small twigs or major branches. However, to ensure the survival of the organism and the long-time reversibility of this type of reconfiguration, breakage should be localized away from the base of the structure [11].

The deformation that an organism can withstand before eventually breaking can be assessed by comparing two material properties: Young's modulus or modulus of elasticity, E, and the yield stress or strength σ_c. The former is the ratio between stress σ and strain ϵ in the material, while the latter characterizes the stress at breakage. The dimensionless number formed out of these two quantities, $\varepsilon_c = \sigma_c/E$, is simply the strain at breakage, or critical strain. Physically, a low value of ε_c means that breakage will occur at small deformations. As seen in fig. 1, the critical strain, ε_c, can differ by several orders of magnitude in organic materials. Yet, terrestrial and benthic organisms are generally submitted to similar flow-induced loads. One may thus wonder how different values of ε_c may affect their mechanical response and their ability to survive in intense flows. The asymptotic limits of brittle materials and highly deformable materials were addressed in previous papers [9,11]. The novelty of the present work is to unify these two approaches within a common framework and to propose a modeling approach valid for any value of the critical strain ε_c.

In this work, we explore, using idealized systems, how the critical strain may select different plant reconfiguration strategies (*i.e.* bending, pruning, or a combination of both). We show that these different strategies lead to comparable drag reductions. In the next section, we present the model for plants and reconfiguration. The results on reconfiguration are then presented first for a single tapered beam, and then for the case of a bundle of tapered beams. Finally, a discussion and conclusion are given in the last section.

(a) Current address: Aix Marseille Université, CNRS, IUSTI UMR 7343 - 13453 Marseille, France; e-mail: diego.lopez@univ-amu.fr

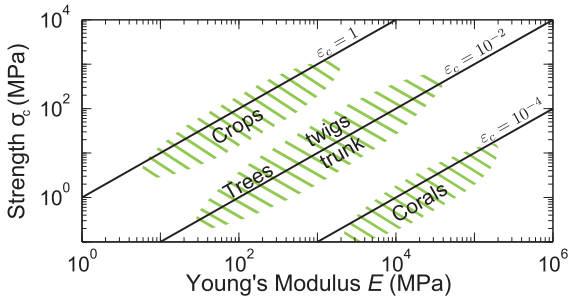

Fig. 1: (Colour on-line) Typical orders of magnitude of Young's modulus and strength in plants and benthic organisms. For crops, the shaded area is centered on values from [13,14]. For trees, this area corresponds to the envelope of multiple data points extracted from [15–20]. The values for corals are estimated from measures on mineral materials like gypsum [21].

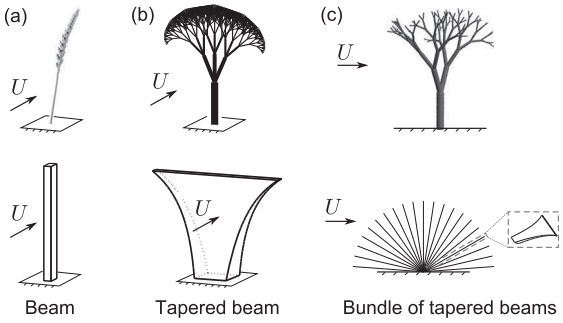

Fig. 2: Typical plant geometries and corresponding models: (a) beam (no ramifications) [14,24]; (b) tapered beam (ramifications, no branch orientation) [12,22]; (c) bundle of tapered beams (ramifications and branch orientation) [25].

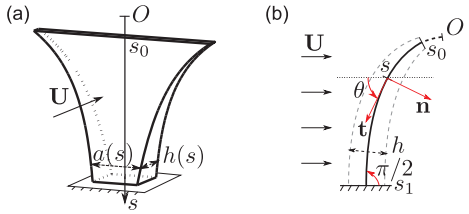

Fig. 3: (Colour on-line) Tapered beam and notations.

Model for plant reconfiguration. – Plants, and more generally slender organisms under flow, are modeled here as cantilever tapered beams, whose width, a, and thickness, h, vary as

$$a(s) = a_0 \left(s/s_1\right)^{\alpha}, \quad h(s) = a_0 \left(s/s_1\right)^{\beta}, \tag{1}$$

where s is the coordinate along the beam axis measured from top ($s = s_0$) to bottom ($s = s_1$), and α, β are slenderness exponents [22]. Here, α characterizes the frontal area and, as such, plays a significant role in the experienced drag. Its influence on the stress distribution is however limited, and so is its impact on the reconfiguration process. Hence, in the following, we present results obtained for $\alpha = -\beta$. This corresponds to constant cross-sectional area, *i.e.* Leonardo's rule [12,23], but we have checked that the conclusions of this Letter remain valid in the general case ($\alpha \neq -\beta$).

The case $\beta = 0$ corresponds to a single-beam plant, with homogeneous width and thickness (*e.g.* cereal crop, fig. 2(a)). When $\beta > 0$, the tapered beam represents a ramified system (fig. 2(b)): the thickness, h, corresponds to the local branch diameter, and the width, a, to the diameter multiplied by the number of branches at that height [22]. The width thus corresponds to the total area facing the flow, or the sail area, thereby neglecting any shading between branches and the effect of branch orientation. To investigate the impact of branch orientation on our results, we finally consider a "bundle" made of several tapered beams of different orientations (fig. 2(c)).

These tapered beams are assumed to lie in a uniform cross-flow of velocity U (fig. 3) such that flow-induced loads (force per unit length), $\mathbf{F}$, resulting from pressure drag read

$$\mathbf{F}(s) = F\,\mathbf{n}, \quad \text{with} \quad F = \frac{1}{2}\rho C_D a \left[U \sin\theta\right]^2, \tag{2}$$

where ρ is the fluid density, $\theta(s)$ is the local beam orientation, and C_D is the drag coefficient, taken to be 1 without loss of generality [4].

Considering the high slenderness of this geometry, beam theory can be used to derive the deflection and stress state along the beam axis (fig. 3(b)). Noting F_t and F_n the tangential and normal components of the internal force, respectively, I the beam's second moment of inertia, and E its Young's modulus, the Euler-Bernoulli beam equation yields

$$F_n' + \theta' F_t + F = 0, \tag{3}$$

$$F_t' - \theta' F_n = 0, \tag{4}$$

$$(EI\theta')' + F_n = 0, \tag{5}$$

where primes stand for differentiation with respect to s [26]. Equations (3)–(5) describe the evolution of internal forces and torques along s, and are solved numerically using a shooting method with a clamped boundary condition at the base, *i.e.* $\theta(s_1) = \pi/2$, and free boundary conditions at the top, *i.e.* $F_t(s_0) = F_n(s_0) = 0$ and $\theta'(s_0) = 0$ (torque-free condition). The total drag is obtained by projecting the internal elastic force evaluated at the base ($s = s_1$) along the flow direction. In the case of the tapered-beam bundle, the total drag is obtained by summing the different beams' contributions. Finally, drag and velocity are normalized so that the drag is 1 when the flow velocity is 1 in the absence of reconfiguration.

In this problem, tangential forces are negligible compared to the normal ones. We therefore focus only on breakage due to bending, and neglect the contribution of compressive and tensile strains induced by the wind [27]. In each cross-section, the bending stresses are maximum at the surface of the beam, being compressive (respectively, extensive) on the downstream side

(respectively, upstream side). The maximum stress is $\sigma_{\max} = E\theta' h/2$ [27], and we assume that breakage occurs when and where $\sigma_{\max} = \sigma_c$. Following a breaking event, the broken part is removed, and s_0 updated [11].

Reconfiguration of a tapered beam. –

Asymptotic limits. Before studying the reconfiguration of a single tapered beam for arbitrary values of ε_c, it is worth investigating two asymptotic limits: brittle materials, $\varepsilon_c \ll 1$ for which breakage occurs before any significant bending, and highly deformable materials, $\varepsilon_c \gg 1$, which essentially never break.

In the classical limit of an elastic material without breaking, $\varepsilon_c \gg 1$, a common behavior is generally observed [10]: for large deformations of the structure, drag increases as $U^{4/3}$, a significant reduction from the U^2 scaling obtained for a rigid structure. This exponent can be obtained considering that the original length scale of the structure does not contribute to the drag when the beam is significantly deformed through bending. In the present problem, this consideration also implies that tapering does not affect the drag either. The 4/3 exponent is then derived directly by scaling analysis, as there are only four physical quantities in the problem, namely the bending rigidity, the drag per unit width, the fluid density and the flow velocity [9]. This drag reduction is consistent with experimental data on many plant species, aquatic or aerial [10]. We thus expect that, in the limit of large critical strain, $\varepsilon_c \gg 1$, drag will vary as $U^{4/3}$ for all β if the flow velocity is large enough.

The limit of a brittle beam, $\varepsilon_c \ll 1$, was considered in ref. [11]. Two different behaviors were identified depending on the value of β. If $\beta < 1$, the flow-induced stress is always maximum at the base, and breaking will systematically occur there. Drag increases as U^2 before breaking occurs. When $\beta > 1$, breaking occurs at an intermediate level, resulting in a succession of breaking events as the flow velocity is increased. The corresponding drag shows sudden reductions, at the breaking events, separated by increases in drag that are quadratic with velocity. This step-by-step process was described as flow-induced pruning, and is relevant for complex tree geometries.

General case. In the general case, when both bending and pruning are involved, it should be noted that flow-induced loads are predominantly exerted on the upper part of the structure (since $a(s)$ diverges as $s \to 0$). As a consequence, the cut-off length s_0 plays a role in scaling the flow-induced loads. In branching structures such as trees, the ratio s_0/s_1 is given by the relative length of the last branches, and can safely be estimated within $10^{-3} < s_0/s_1 < 10^{-1}$ for most organic branched structures [28]. In the following, we consider a typical value of this ratio $s_0/s_1 = 10^{-2}$.

We now investigate the reconfiguration through bending and pruning of a single tapered beam when the flow velocity is gradually increased. We focus here on the case $\beta > 1$ for which intermediate breaking events (*i.e.* pruning) are possible. A typical value is $\beta = 3/2$ as proposed by McMahon and Kronauer [28] based on the principle of elastic similarity in trees (the case $\beta < 1$ will be discussed below).

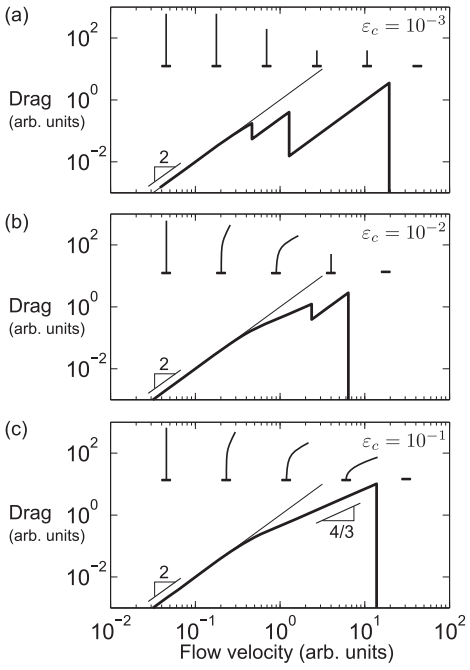

Fig. 4: Evolution of the normalized drag as a function of the flow velocity, for a tapered beam ($\beta = 3/2$): (a) pruning reconfiguration, $\varepsilon_c = 10^{-3}$; (b) bending and pruning, $\varepsilon_c = 10^{-2}$; (c) bending reconfiguration, $\varepsilon_c = 10^{-1}$. The drag evolution in the absence of reconfiguration is shown as a thin line; beam topologies are sketched for different flow velocities.

Figure 4 shows the computed drag on a tapered beam as the flow velocity is increased. Three values of the critical strain are considered: $\varepsilon_c = 10^{-3}$, 10^{-2}, and 10^{-1}. Regardless of ε_c, drag is significantly reduced in comparison with a rigid body. Also, despite fundamental differences in the reconfiguration mechanisms, the resulting magnitude of drag reduction is comparable. At low critical strain, $\varepsilon_c = 10^{-3}$, little bending occurs, and reconfiguration is essentially due to pruning (fig. 4(a)). This case is representative of fragile materials for which $\varepsilon_c \ll 1$. Conversely, at large critical strain, $\varepsilon_c = 10^{-1}$, reconfiguration is essentially driven by bending, until pruning eventually occurs through a single breaking event, at the base of the structure (fig. 4(c)). This regime is reminiscent of highly deformable materials, $\varepsilon_c \gg 1$, except that the finite value of ε_c selects a flow velocity at which the structure breaks. Before breaking occurs, the asymptotic bending regime of drag reduction described above is found, where drag varies as $U^{4/3}$. In the intermediate case, $\varepsilon_c = 10^{-2}$, reconfiguration and drag reduction are achieved through first bending and then pruning (fig. 4(b)).

Reconfiguration of a bundle of tapered beams. – From the reconfiguration of a single tapered beam, we see that both bending and pruning yield important and comparable drag reductions. To assess the importance of

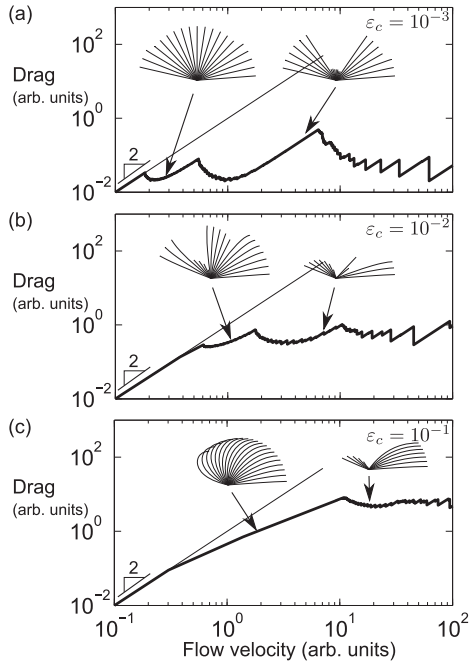

Fig. 5: Evolution of the normalized drag as a function of the flow velocity, for a radial bundle of tapered beams ($\beta = 3/2$): (a) $\varepsilon_c = 10^{-3}$, (b) $\varepsilon_c = 10^{-2}$ and (c) $\varepsilon_c = 10^{-1}$. The drag evolution in the absence of reconfiguration is shown as a thin line, and the bundle topologies are sketched for different reconfigured states.

branch orientations, we now model the reconfiguration of a bundle of such beams (fig. 2(c)). This geometry is inspired from the poroelastic system of ref. [25], where the authors considered the purely elastic case. It can be seen as a model for bushes or tree crowns, as each beam can itself be interpreted as a ramified branch. Although shading by upstream beams is likely to impact the total drag, ref. [25] showed that accounting for an associated pressure loss did not modify significantly the reconfiguration laws. For simplicity, we present here the worst case scenario, where shading effects are neglected and each beam experiences the same flow velocity.

Figure 5 shows the evolution of the drag on the bundle geometry when flow velocity is increased. Depending on the value of ε_c, the topology of the reconfiguration is quite different. For low critical strain, $\varepsilon_c = 10^{-3}$, breakage propagates from the center of the bundle to its periphery. For high critical strain, $\varepsilon_c = 10^{-1}$, breakage propagates downstream. For moderate critical strain, $\varepsilon_c = 10^{-2}$, the behavior is a combination of these two propagative scenarios, leading to non-trivial reconfiguration patterns. Yet, these different scenarios share similar trends in the drag reduction, and the existence of a bound on the experienced drag (at fixed ε_c) can be identified. Although this bound depends on the value of ε_c, this dependence is mostly due to the normalization chosen rather than a biological property. This confirms the results obtained for a single beam, suggesting that different values of the critical strain, and hence different reconfiguration strategies, provide the structure with similar abilities to survive under extreme flows. Furthermore, regardless of the reconfiguration mechanism, the combination of identical elements with different orientations appears as a powerful mean for maintaining the drag bounded as flow velocity increases.

Additionally, the shape after reconfiguration of the present bundle shares some similarities with flag trees, a morphology observed on some species of trees growing in extreme winds. For these trees, it has been recognized that abrasion plays a central role in determining the shape, by removing upstream branches [29]. Using our bundle model for large critical strains typical of growing wood, we see that the upwind-facing branches would be the first to break (fig. 5(c)). This would result in a tree with most branches oriented downwind similarly to flag trees. Such hypothesis could be validated by coupling the present model with a tree growth model.

Discussion and conclusion. – Using model geometries, we have shown how different reconfiguration strategies (bending, pruning, or a combination of both) ensure drag reduction and survival under important fluid flows. Starting from the observation that critical strains measured in nature vary by several orders of magnitude, we have focused on the effect of this mechanical parameter on reconfiguration. We have shown that the evolution of drag with flow velocity is similar for any value of the critical strain. In particular, taking into account the variety of branch orientations, as a model of ramified plants, the drag appears bounded for a given critical strain. Such a remarkable property could balance efficiently the high biological cost of pruning.

In this work, we focused on the reduction of flow-induced drag associated with different mechanisms, regardless of the biological cost for the plant. The cost of reconfiguration is difficult to define in a unique way. Flow-induced pruning is indeed expensive due to the important loss of biomass, whereas bending seems cost-free. However, a branch breakage results in a permanent drag reduction, as opposed to bending, where successive elastic deformations yield fatigue and growth modifications. Additionally, pruning helps removing weaker parts of the plant, and is therefore part of the growth process aiming at developing more resistant structures.

The results shown above were obtained for a slenderness exponent β larger than 1. For beam-like plants (*i.e.* without tapering, $\beta \approx 0$), such as cereal crops and many annual plants, there can only be a single breaking event at the base since $\beta < 1$. This scenario is also true for young trees that do not have enough branching levels for branch breakage to occur [11]. In this case, reconfiguration relies only on bending, and the corresponding drag curves are reduced to that computed at the highest critical strain, $\varepsilon_c = 0.1$, in figs. 4 and 5. Note that, because β does not influence how drag scales with velocity in these highly bent regimes, these curves also represent the case $\beta < 1$.

Table 1: Typical survival strategy to resist large flow-induced loads and corresponding value of the critical strain ε_c for different natural structures.

Structure	Strategy	ε_c
Corals [21]	base breakage and reattachment	10^{-4}
Trees [15,16,20]		
branches	bending/ pruning and regrowth	10^{-2}
twigs	bending	10^{-1}
Crops [14]	bending	10^{-1}

When $\beta < 1$, pruning is not a possible reconfiguration mechanism. It suggests that low critical strain is not favorable in that case. This is consistent with the observations: crops are indeed annual plants whose critical strain is high, and young trees have different mechanical properties than old trees, with more flexible branches and smaller Young's moduli [16]. For instance, in the young walnut tree analyzed in [30], β was lower than 1, $\beta \approx 0.82$, and Young's modulus was lower than that of older trees, suggesting a possible higher value of the critical strain. This beneficial property could result from an evolutionary process, as proposed for perennial kelp [31]. The particular case of stony corals is also noteworthy, as they have a very low critical strain, $\varepsilon_c \approx 10^{-4}$. Their geometry, where the sections of branches are similar to that of the trunk, suggests that breakage will occur at their base [21,32,33]. However, these particular organisms are capable of reattachment after breakage, thus ensuring their survival through breakage and dispersal. This is also a common mechanism for asexual reproduction in some terrestrial plants like *Salix* [15,21]. This ability to reattach can be seen as the ultimate survival strategy when neither bending nor pruning work.

Hence slender organisms subjected to flow may survive to extreme loading, regardless of the critical strain of the material they are made of, by one mechanism or another, or a combination of them (table 1). This result suggests that the choice of either reconfiguration mechanism is not driven by survival issues, but probably related to other plant functionalities. This allows a large variety of states of living materials and geometries to exist in such environments, as is commonly observed [6,16]. More generally, these drag reduction strategies through shape changes may be seen as one of the posture controls of plants, in reaction to an abiotic stress, see, for instance, in [1,34].

REFERENCES

[1] Moulia B., Coutand C. and Lenne C., *Am. J. Bot.*, **93** (2006) 1477.

[2] Telewski F. W., *Am. J. Bot.*, **93** (2006) 1466.

[3] Vogel S., *Am. Zool.*, **24** (1984) 37.

[4] de Langre E., *Annu. Rev. Fluid Mech.*, **40** (2008) 141.

[5] Vogel S., *J. Exp. Bot.*, **40** (1989) 941.

[6] Koehl M. A. R., *Am. Zool.*, **24** (1984) 57.

[7] Kane B., Pavlis M., Harris J. R. and Seiler J. R., *Can. J. Forest Res.*, **38** (2008) 1275.

[8] Alben S., Shelley M. and Zhang J., *Nature*, **420** (2002) 479.

[9] Gosselin F., de Langre E. and Machado-Almeida B. A., *J. Fluid Mech.*, **650** (2010) 319.

[10] de langre E., Gutierrez A. and Cossé J., *C. R. Méc.*, **340** (2012) 35.

[11] Lopez D., Michelin S. and de Langre E., *J. Theor. Biol.*, **284** (2011) 117.

[12] Eloy C., *Phys. Rev. Lett.*, **107** (2011) 258101.

[13] Crook M. J., Ennos A. R. and Sellers E. K., *J. Exp. Bot.*, **45** (1994) 857.

[14] Baker C., *J. Theor. Biol.*, **175** (1995) 355.

[15] Beismann H., Wilhelmi H., Baillères H., Spatz H. C., Bogenrieder A. and Speck T., *J. Exp. Bot.*, **51** (2000) 617.

[16] Speck T. and Burgert I., *Annu. Rev. Mater. Res.*, **41** (2011) 169.

[17] Rosner S., Klein A., Muller U. and Karlsson B., *Tree Physiol.*, **27** (2007) 1165.

[18] Bjurhager I., Berglund L., Bardage S. and Sundberg B., *J. Wood Sci.*, **54** (2008) 349.

[19] Butler D. W., Gleason S. M., Davidson I., Onoda Y. and Westoby M., *New Phytol.*, **193** (2012) 137.

[20] Gibson L. J., *J. R. Soc. Interface*, **9** (2012) 2749.

[21] Tunnicliffe V., *Proc. Natl. Acad. Sci. U.S.A.*, **78** (1981) 2427.

[22] McMahon T. A., *Sci. Am.*, **233** (1975) 93.

[23] Lindenmayer A. and Prusinkiewicz P., *The Algorithmic Beauty of Plants* (Springer-Verlag) 1996.

[24] Luhar M. and Nepf H. M., *Limnol. Oceanogr.*, **56** (2011) 2003.

[25] Gosselin F. P. and de Langre E., *J. Fluids Struct.*, **27** (2011) 1111.

[26] Salençon J., *Handbook of Continuum Mechanics: General Concepts, Thermoelasticity* (Springer) 2001.

[27] Niklas K. J., *Plant Biomechanics: An Engineering Approach to Plant Form and Function* (University of Chicago Press, Chicago, Ill., USA) 1992.

[28] McMahon T. A. and Kronauer R. E., *J. Theor. Biol.*, **59** (1976) 443.

[29] Telewski F. W., *Science*, **184** (2012) 20.

[30] Rodriguez M., de Langre E. and Moulia B., *Am. J. Bot.*, **95** (2008) 1523.

[31] Demes K. W., Pruitt J. N., Harley C. D. and Carrington E., *Funct. Ecol.*, **27** (2013) 439.

[32] Highsmith R. C., *Mar. Ecol. Prog. Ser.*, **7** (1982) 207.

[33] Madin J. S., *Coral Reefs*, **24** (2005) 630.

[34] Bastien R., Bohr T., Moulia B. and Douady S., *Proc. Natl. Acad. Sci. U.S.A.*, **110** (2013) 755.